Elastodynamic analysis by a frequency-domain FEM-BEM iterative coupling procedure

Delfim Soares Jr.[*1], Kleber A. Gonçalves[2a] and José Claudio de Faria Telles[2b]

[1]*Structural Engineering Department, Federal University of Juiz de Fora, CEP 36036-330, Juiz de Fora, Brazil*
[2]*Department of Civil Engineering, Federal University of Rio de Janeiro, CEP 21945-970, Rio de Janeiro, Brazil*

Abstract. This paper presents a coupled FEM-BEM strategy for the numerical analysis of elastodynamic problems where infinite-domain models and complex heterogeneous media are involved, rendering a configuration in which neither the Finite Element Method (FEM) nor the Boundary Element Method (BEM) is most appropriate for the numerical analysis. In this case, the coupling of these methodologies is recommended, allowing exploring their respective advantages. Here, frequency domain analyses are focused and an iterative FEM-BEM coupling technique is considered. In this iterative coupling, each sub-domain of the model is solved separately, and the variables at the common interfaces are iteratively updated, until convergence is achieved. A relaxation parameter is introduced into the coupling algorithm and an expression for its optimal value is deduced. The iterative FEM-BEM coupling technique allows independent discretizations to be efficiently employed for both finite and boundary element methods, without any requirement of matching nodes at the common interfaces. In addition, it leads to smaller and better-conditioned systems of equations (different solvers, suitable for each sub-domain, may be employed), which do not need to be treated (inverted, triangularized etc.) at each iterative step, providing an accurate and efficient methodology.

Keywords: elastodynamics; frequency domain; iterative coupling; relaxation parameter

1. Introduction

The numerical simulation of arbitrarily shaped continuous bodies subjected to harmonic or transient loads remains, despite much effort and progress over the last decades, a challenging area of research. In most cases, discrete techniques, such as the finite element method (FEM) and the boundary element method (BEM) have been employed and continuously further developed with respect to accuracy and efficiency. Both methodologies can be formulated in the time domain or in the frequency domain, and each approach has relative benefits and limitations. The finite element method, for instance, is well suited for inhomogeneous and anisotropic materials as well as for dealing with the nonlinear behaviour of a body. For systems with infinite extension and regions of high stress concentration, however, the use of the boundary element method is by far more

---

∗Corresponding author, D.Sc., E-mail: delfim.soares@ufjf.edu.br
[a] D.Sc. Student, E-mail: kleber.a.g@hotmail.com
[b] Ph.D., E-mail: telles@coc.ufrj.br

advantageous.

In fact, it did not take long until some researchers started to combine the FEM and the BEM in order to profit from their respective advantages, trying to evade their disadvantages, and nowadays several works dealing with FEM-BEM coupling are available (an overview is provided by Beskos 2003, taking into account dynamic analyses). However, standard coupling procedures of FEM/BEM can lead to several problems with respect to efficiency, accuracy and flexibility. First, the coupled system of equations has a banded symmetric structure only in the FEM part, while in the BEM part it is non-symmetric and fully populated. Consequently, for its solution, the optimized solvers usually used by the FEM cannot be employed anymore, which leads to rather expensive calculations with respect to computer time. Second, quite different physical properties may be involved in the coupled model, resulting in bad-conditioned matrices when standard coupling procedures are considered. This may affect the accuracy of the methodology, providing misleading results. Third, the standard coupling methodology does not allow independent discretization for each sub-domain of the model, requiring matching nodes at common interfaces, which drastically affects the flexibility and versatility of the technique.

In order to evade these drawbacks, iterative coupling procedures have been developed. Initially, static problems were studied considering iterative coupling approaches, and linear and nonlinear behaviour have been simulated (Lin *et al.* 1996, Elleithy *et al.* 2001, 2009, 2012, Jahromi *et al.* 2009, Boumaiza and Aour 2014). Later on, dynamic problems were focused, and time domain analyses were initially implemented (Soares *et al.* 2004, Soares 2008, 2012). Recently, frequency domain iterative analyses have also been considered; but, in this case, most works are related to fluid-fluid or fluid-structure coupled models (Bendali *et al.* 2007, Soares and Godinho 2012, Godinho and Soares 2013). For an overview of recent advances in the iterative analysis of coupled models considering time and frequency domain approaches, the work of Soares and Godinho 2014 is recommended. Other domain decomposition approaches are also available nowadays, based on different techniques, such as those presented by Bernardi *et al.* 1990 and Belgacem 1999 (considering mortaring techniques), Gosselet and Rey 2006 (presenting a review of most employed approaches and their strong connections), Vion and Guezaine 2014 (presenting a preconditioner for non-overlapping Schwarz methods applied to the Helmholtz problem) etc..

Iterative coupling approaches allow BEM and FEM sub-domains to be analyzed separately, leading to smaller and better-conditioned systems of equations (different solvers, suitable for each sub-domain, may be employed). Moreover, a small number of iterations is required for the algorithm to converge and the matrices related to the smaller governing systems of equations do not need to be treated (inverted, triangularized etc.) at each iterative step, providing an efficient methodology. This coupling technique allows independent discretizations to be efficiently employed for the boundary and finite element sub-domains, without any requirement of matching nodes at the common interfaces. As a matter of fact, in the present work, constant boundary elements and linear finite elements are considered, and matching functional nodes are never provided in the common interfaces. It is important to observe, however, that frequency domain analyses usually give rise to ill-posed problems and, in these cases, the convergence of the iterative coupling algorithm can be either too slow or unachievable if no special procedure is taken into account. In order to deal with this ill-posed problem and ensure convergence of the iterative coupling algorithm, an optimal iterative procedure is adopted here, with optimal relaxation parameters being computed at each iterative step. Thus, an expression to compute optimal relaxation parameters, which is quite efficient and easy to implement, is provided and discussed, being its effectiveness illustrated at the end of the paper, where numerical examples are analyzed.

In the numerical examples, soil-structure interacting models are discussed, being the results of the proposed iterative coupling formulation compared to those of the standard coupling technique. As one will observe, the proposed technique is flexible, robust and efficient, allowing a quite effective coupling of the finite element and boundary element methods for frequency domain elastodynamic analyses.

2. Governing equations

The frequency domain elastic wave equation for homogenous media is given by

$$\rho\left(c_d^2 - c_s^2\right)u_j(X,\omega)_{,ji} + \rho c_s^2 u_i(X,\omega)_{,jj} + (\omega^2\rho - i\omega v)u_i(X,\omega) + b_i(X,\omega) = 0 \tag{1}$$

where $u_i(X,\omega)$ and $b_i(X,\omega)$ stand for the displacement and the body force distribution components, respectively. In Eq. (1), c_d is the dilatational wave velocity and c_s is the shear wave velocity, they are given by: $c_d^2 = (\lambda + 2\mu)/\rho$ and $c_s^2 = \mu/\rho$, where ρ is the mass density and λ and μ are the Lamé's constants. v stands for viscous damping related parameters. Eq. (1) can be obtained from the combination of the following basic mechanical equations (proper to model heterogeneous media)

$$\sigma_{ij}(X,\omega)_{,j} + \left(\rho(X)\omega^2 - i\omega v(X)\right)u_i(X,\omega) + b_i(X,\omega) = 0 \tag{2a}$$

$$\sigma_{ij}(X,\omega) = \lambda(X)\delta_{ij}\varepsilon_{kk}(X,\omega) + 2\mu(X)\varepsilon_{ij}(X,\omega) \tag{2b}$$

$$\varepsilon_{ij}(X,\omega) = (1/2)(u_i(X,\omega)_{,j} + u_j(X,\omega)_{,i}) \tag{2c}$$

where $\sigma_{ij}(X,\omega)$ and $\varepsilon_{ij}(X,\omega)$ are, respectively, stress and strain tensor components, and δ_{ij} is the Kronecker delta $(\delta_{ij} = 1, \text{for } i = j \text{ and } \delta_{ij} = 0, \text{for } i \neq j)$. Eq. (2(a)) is the momentum equilibrium equation; Eq. (2(b)) represents the constitutive law of the linear elastic model and Eq. (2(c)) stands for kinematical relations. The boundary conditions of the elastodynamic problem are given by

$$u_i(X,\omega) = \bar{u}_i(X,\omega) \text{ for } X \in \Gamma_1 \tag{3a}$$

$$\tau_i(X,\omega) = \sigma_{ij}(X,\omega)n_j(X) = \bar{\tau}_i(X,\omega) \text{ for } X \in \Gamma_2 \tag{3b}$$

where the prescribed values are indicated by over bars, $\tau_i(X,\omega)$ denotes the traction vector along the boundary and $n_j(X)$ stands for the components of the unit outward normal vector.

3. Boundary element modeling

The BEM integral equation related to the elastodynamic model is given by

$$\tag{4}$$
$$c_{ij}(\xi)u_j(\xi,\omega) = \int_\Gamma u_{ij}^*(X;\xi,\omega)\tau_j(X,\omega)\, d\Gamma - \int_\Gamma \tau_{ij}^*(X;\xi,\omega)\, u_j(X)\, d\Gamma + \varsigma_i(X;\xi,\omega)$$

where $c_{ij}(\xi)$ depends on geometric aspects, $\varsigma_i(X; \xi, \omega)$ stands for possible domain integral contributions (such as body sources) and the terms $u_{ij}^*(X; \xi, \omega)$ and $\tau_{ij}^*(X; \xi, \omega)$ represent the fundamental displacement and traction, respectively (X is the field point and ξ is the source point). For a two-dimensional approach, the fundamental solutions can be found at Dominguez (1993).

By introducing spatial approximations for the variables of the model into the integral Eq. (4), the following system of equations can be obtained, once proper numerical treatment is considered (Dominguez 1993)

$$CU(\omega) = G(\omega)T(\omega) - H(\omega)U(\omega) + S(\omega) \tag{5}$$

where C, G and H are influence matrices, S is a vector related to domain integrals and U and T are displacement and traction vectors, respectively, at frequency ω. After considering the boundary conditions of the problem (translating all the known variables to the right-hand-side of Eq. (5), and the unknown fields to the left-hand-side), the BEM responses for the elastic model can be computed for the given frequency ω.

4. Finite element modelling

The integral weak-form of the governing equations at section 2 can be written as

$$\tag{6}$$

$$-\omega^2 \int_\Omega \rho(X)u_i(X, \omega)w_{ik}(X)d\Omega + i\omega \int_\Omega \nu(X)u_i(X, \omega)w_{ik}(X)d\Omega +$$

$$+ \int_\Omega \sigma_{ij}(X, \omega)w_{ik}(X)_{,j}d\Omega + \int_\Omega b_i(X, \omega)w_{ik}(X)d\Omega - \int_{\Gamma_2} \tau_i(X, \omega)w_{ik}(X)d\Gamma = 0$$

where $w_{ik}(X)$ stands for a weight function, which is assumed to have null values in the essential boundary (i.e., $w_{ik}(X) = 0$ for $X \in \Gamma_1$).

By introducing spatial approximations for the variables of the model into the integral Eq. (6), and by adopting these approximations to define the specified weight functions (Galerkin Method), the following system of equations can be obtained, once proper numerical treatment is considered (Bathe 1996, Hughes 2000)

$$-\omega^2 MU(w) + i\omega CU(\omega) + KU(\omega) = F(\omega) \tag{7}$$

where M, C and K stand for the mass, damping and stiffness matrix of the model, respectively, and U and F stand for the nodal displacement and force vector, respectively. Matrices M, C and K are computed taking into account the first, second and third terms in Eq. (6), respectively, whereas vector F is computed taking into account the last two terms in the l.h.s. of Eq. (6) (for the stiffness matrix computation, Eqs. (2(b)) and (2(c)) are employed to relate the stress tensor with the displacement vector). After considering the boundary conditions of the problem, the FEM responses for the elastodynamic model can be computed for the given frequency ω, taking into account Eq. (7).

5. Coupling procedures

In order to enable the coupling between the BEM and the FEM sub-domains of the model, an iterative procedure is employed here, which performs a successive update of the relevant variables at the common interfaces. The proposed approach is based on the imposition of prescribed displacement at the BEM sub-domain and of prescribed nodal forces at the FEM sub-domain. Since the two sub-domains are analysed separately, the relevant systems of equations are formed independently, before the iterative process starts, and are kept constant for each frequency along the iterative process. The separate treatment of the two sub-domains allows independent discretizations to be used on both parts, without any special requirement of matching nodes along the common interfaces. Thus, the coupling algorithm can be presented for a generic case, in which the interface nodes may not match, allowing exploiting this benefit of the iterative coupling formulation.

To ensure and/or to speed up convergence, a relaxation parameter λ is introduced in the iterative coupling algorithm. The effectiveness of the iterative process is strongly related to the selection of this relaxation parameter, since an inappropriate selection for λ can significantly increase the number of iterations in the analysis or, even worse, make convergence unfeasible. At the end of the section, an optimal relaxation parameter is calculated, taking into account the coupled BEM-FEM frequency-domain formulation.

5.1 Iterative coupling procedures

Initially, in the kth iterative step of the FEM-BEM coupling, the FEM sub-domain is analysed and the structure displacements at the common interfaces $_f\boldsymbol{U}_I^{(k)}(\omega)$ (subscript I indicates the common interface, whereas f and b indicates finite and boundary element sub-domains, respectively) are computed, as described in section 4. In this case, $_f\boldsymbol{U}_I^{(k)}(\omega)$ is evaluated taking into account prescribed nodal forces at the common interfaces $_f\boldsymbol{F}_I^{(k)}$, which are provided from the previous iterative step (in the first iterative step, null prescribed nodal forces are considered). Once $_f\boldsymbol{U}_I^{(k)}(\omega)$ is computed, it is applied to evaluate the essential boundary conditions that are prescribed at the common interfaces of the BEM sub-domains. More precisely, $_f\boldsymbol{U}_I^{(k)}(\omega)$ is used to compute BEM displacements, as indicated below

$$_b\boldsymbol{U}_I^{(k+\lambda)}(\omega) = \int\limits_{\Gamma_I} \boldsymbol{\delta}^T(X - {_b}X) \, {_f}\boldsymbol{N}(X)d\Gamma \, {_f}\boldsymbol{U}_I^{(k)}(\omega) \tag{8}$$

where $\boldsymbol{\delta}$ stands for a matrix representation of the Dirac's Delta function, employed here just to properly indicate the computation of the variables at the BEM nodes $_bX$, and $\boldsymbol{N}(X)$ stands for the BEM or FEM interpolation functions, according to the subscript b or f, respectively.

To better describe the proposed FEM-BEM coupling methodology, Fig. 1 illustrates its application for the case of constant boundary elements and linear triangular finite elements.

As previously discussed, in this work, relaxation parameters are considered in order to ensure and/or to speed up the convergence of the iterative process. Thus, the displacements $_b\boldsymbol{U}_I^{(k+\lambda)}$ that are calculated by Eq. (8) are actualized as follow
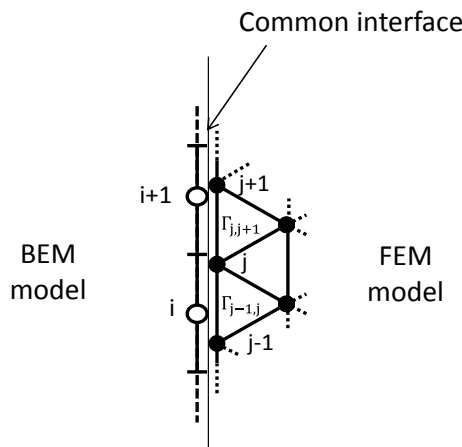
Fig. 1 Detail of a portion of the FEM-BEM interface when linear triangular finite elements and constant boundary are used. In the figure, $j - 1$, j and $j + 1$ are FEM interface nodes, while i and $i + 1$ are BEM nodes. Displacements at BEM node i can be computed by interpolation of FEM displacements at nodes $j - 1$ and j (Eq. (8)); FEM nodal force in j can be calculated by integration of the traction along boundaries $\Gamma_{j-1,j}$ and $\Gamma_{j,j+1}$, using Eq. (10) and considering FEM linear and BEM piecewise constant shape functions along these boundaries

$$_b\boldsymbol{U}_I^{(k+1)}(\omega) = (\lambda) \, _b\boldsymbol{U}_I^{(k+\lambda)}(\omega) + (1 - \lambda) \, _b\boldsymbol{U}_I^{(k)}(\omega) \tag{9}$$

where λ stands for the relaxation parameter.

Once the BEM displacements at the common interfaces are computed, the BEM sub-domains can be analyzed, as described in section 3. As a consequence, the BEM tractions at the common interfaces are evaluated $_b\boldsymbol{T}_I^{(k+1)}$, allowing the computation of the natural boundary conditions that are prescribed at the FEM sub-domains at the next iterative step. This is carried out as indicated below

$$_f\boldsymbol{F}_I^{(k+1)}(\omega) = \int_{\Gamma_I} \, _f\boldsymbol{N}^T(X) \, _b\boldsymbol{N}(X)d\Gamma \, _b\boldsymbol{T}_I^{(k+1)}(\omega) \tag{10}$$

Once $_f\boldsymbol{F}_I^{(k+1)}(\omega)$ is computed, the algorithm goes on to the next iterative step, repeating all the above described procedures, until convergence is achieved.

As it is illustrated in section 6, a proper selection for λ at each iterative step is extremely important for the effectiveness of the iterative coupling procedure. In order to obtain an easy to implement, efficient and effective expression for the relaxation parameter computation, in the next sub-section optimal λ values are deduced.

5.2 Optimal relaxation parameter

In order to evaluate an optimal relaxation parameter, the following square error functional is minimized here

$$f(\lambda) = \left\| \, _bU_I^{(k+1)}(\lambda) - \, _bU_I^{(k)}(\lambda) \right\|^2 \tag{11}$$

where $\, _bU_I$ stands for the BEM prescribed values at the common interfaces.

Taking into account the relaxation of the prescribed values for the $(k+1)$ and (k) iterations, Eqs. (12(a)) and (12(b)) may be written, based on the definition in Eq. (9)

$$_bU_I^{(k+1)} = (\lambda) \, _bU_I^{(k+\lambda)} + (1-\lambda) \, _bU_I^{(k)} \tag{12a}$$

$$_bU_I^{(k)} = (\lambda) \, _bU_I^{(k+\lambda-1)} + (1-\lambda) \, _bU_I^{(k-1)} \tag{12b}$$

Substituting Eqs. (12) into Eq. (11) yields

$$f(\lambda) = \left\| (\lambda)W^{(k+\lambda)} + (1-\lambda) \, W^{(k)} \right\|^2 = \tag{13}$$

$$= (\lambda^2) \left\| W^{(k+\lambda)} \right\|^2 + 2\lambda(1-\lambda)\left(W^{(k+\lambda)}, W^{(k)} \right) + (1-\lambda)^2 \left\| W^{(k)} \right\|^2$$

where the inner product definition is employed (e.g., $(W, W) = \|W\|^2$) and new variables, as defined in Eq. (14), are considered.

$$W^{(k+\lambda)} = \, _bU_I^{(k+\lambda)} - \, _bU_I^{(k+\lambda-1)} \tag{14}$$

To find the optimal λ that minimizes the functional $f(\lambda)$, Eq. (13) is differentiated with respect to λ and the result is set to zero, as described below

$$\lambda \left\| W^{(k+\lambda)} \right\|^2 + (1-2\lambda) \left(W^{(k+\lambda)}, W^{(k)} \right) + (\lambda-1) \left\| W^{(k)} \right\|^2 = 0 \tag{15}$$

Re-arranging the terms in Eq. (15), yields

$$\lambda = \frac{\left(W^{(k)}, W^{(k)} - W^{(k+\lambda)} \right)}{\left\| W^{(k)} - W^{(k+\lambda)} \right\|^2} \tag{16}$$

which is an easy to implement expression that provides an optimal value for the relaxation parameter λ, at each iterative step. This expression requires a low computational cost, when compared to other alternatives that can be found in the literature (see, for instance, Elleithy *et al.* 2001).

Additionally, one should keep in mind that the computed relaxation parameter is a complex number, since the problem is formulated in the frequency domain. This complex number computation could be ranged (e.g., imposing $|\lambda| \leq 1$), but the authors have observed that faster convergence is usually achieved in the iterative process if a non-restricted relaxation parameter selection, provided by Eq. (16), is considered. Moreover, although the authors found that the iterative process is relatively insensitive to the value of the relaxation parameter used for the first step, in all the cases discussed here, a real value of $\lambda = 0.5$ is considered.

6. Numerical analysis

In order to illustrate the performance and potentialities of the discussed techniques, two application examples are considered here, corresponding to a circular ring-shaped structure involved by an infinite soil domain. Different material properties, as well as prescribed load/displacement configurations, are considered in the analyses.

6.1 Ring-shaped structure inside an infinite elastic domain

Consider a circular homogeneous ring-shaped elastic inclusion, inside a homogeneous and infinite elastic environment (see Fig. 2(a)). The external environment has a density of $7,85 \times 10^3$ kg/m^3, Young's modulus of $20,58 \times 10^{10}$ N/m^2 and Poisson's ratio of 0.2 (no damping is considered). This elastic material allows dilatational and shear waves to travel at $5397,17$ m/s and $3305,08$ m/s, respectively. The circular inclusion has an external radius of 3.0 m and an internal radius of 2.0 m and is made of the same elastic material of the external domain.

The external environment is discretized by boundary elements distributed uniformly along the common interface (straight boundary elements with constant interpolation functions are adopted); the ring structure is modelled by using linear triangular finite elements. Fundamental harmonic displacements are prescribed at the internal cavity of the ring structure, which are acquired by considering a horizontal Dirac's delta force acting at the centre of the cavity. Thus, the analytical solution for the problem is known and it is provided by the model's fundamental solutions.

First, the external environment is modelled using 40 boundary elements, while a total of 210 elements (40 nodes at the interface) are considered at the finite element mesh. The corresponding FEM and BEM discretizations are illustrated in Figs. 2(b) and 2(c), respectively.

Fig. 3 illustrates the displacements computed at point A (see Fig. 2(a)), taking into account the proposed iterative coupling procedure, considering a frequency range from 100 to 5000 Hz. Analytical answers and results computed taking into account a standard FEM-BEM direct coupling methodology are also depicted in Fig. 3, for comparison. As one can observe, the results provided by these different approaches are in good agreement. It is important to highlight that the coupled FEM-BEM results get closer to the analytical answers as the discretization of the model is refined.
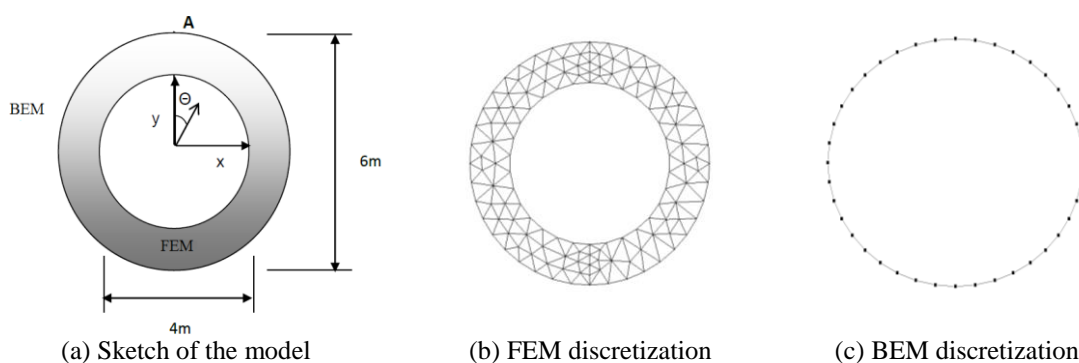

(a) Sketch of the model   (b) FEM discretization   (c) BEM discretization

Fig. 2 Model's sketch and discretization

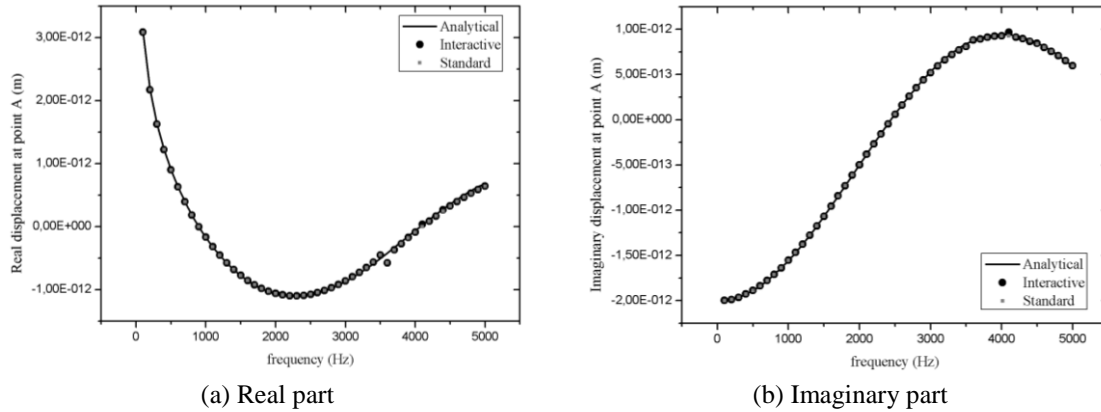(a) Real part   (b) Imaginary part

Fig. 3 Vertical displacements at point A

Table 1 Discretizations for the BEM and FEM sub-domains

BEM	FEM
straight constant elements	triangular linear elements
Mesh 1: 20 elements	Mesh 1: 162 elements (20 elements at the interface)
Mesh 2: 40 elements	Mesh 2: 210 elements (40 elements at the interface)
Mesh 3: 80 elements	Mesh 3: 726 elements (80 elements at the interface)
Mesh 4: 160 elements	Mesh 4: 3436 elements (160 elements at the interface)

As a matter of fact, the convergence of the proposed technique is analyzed next, taking into account independent discretizations (and, as a consequence, no matching nodes at the common interface) for the FEM and the BEM. In order to do so, 4 discretizations for the BEM sub-domain and 4 discretizations for the FEM sub-domain are focused, as described in Table 1 (as one may observe, meshes 2 are those depicted in Fig. 2). These different discretizations are combined among each other and the errors that arise (taking into account the analytical answer of the model) are depicted in Fig. 4. Three combinations are considered here, the first one considers the FEM mesh 4 (i.e., 160 nodes on the FEM common interface) combined with all the focused BEM meshes. This combination is referred here as "FEM 160 / BEM". The second combination considers the BEM mesh 4 (i.e., 160 nodes on the BEM common interface) combined with all the focused FEM meshes. This combination is referred here as "BEM 160 / FEM". Finally, standard node-to-node combinations (i.e., considering matching geometrical nodes at the common interface) of the BEM and FEM meshes are also considered, and this combination is referred here as "node / node".

The relative errors depicted in Fig. 4 are computed as follows

$$E = \sqrt{\frac{\sum_{i=1}^{nf}[(|\ ^{i}U_c\ |) - (|\ ^{i}U_a\ |)]^2}{\sum_{i=1}^{nf}(|\ ^{i}U_a\ |)^2}} \tag{17}$$

where $^{i}U_c$ stands for the computed numerical displacement at point A and frequency i, $^{i}U_a$ stands for the analytical answer at the same point and frequency, and nf is the total number of frequencies considered in the analysis.

As one can observe in Fig. 4(a), convergence is achieved, even considering non-matching nodes at the common interface. As it can be further observed in Fig. 4a, the "BEM 160 / FEM" and the "node / node" curves are very close, indicating that, in this case, a small amount of boundary elements are sufficient to properly discretize the model. On the other hand, better results are obtained considering the "FEM 160 / BEM" combination, which was expected, since refined FEM discretizations can better represent the prescribed boundary conditions of the model, providing more accurate analyses.

In Fig. 4(b), the computed errors are plotted against the CPU times of the analyses. As one can observe, considering matching nodes at the common interface, the iterative coupling procedure is usually more efficient than the standard direct coupling procedure (i.e., for a given CPU time of analysis, more accurate results can be obtained by the iterative procedure; or, for a given accuracy level, faster analyses can be provided by the iterative procedure). Moreover, as described in Fig. 4(a), once proper discretizations are considered for each sub-domain of the model, even more efficient analyses may be achieved, highlighting the importance of a coupling procedure that allows flexible and independent discretizations of the involved sub-domains, taking into account non-matching nodes at the common interfaces.

In order to further analyze the performance of the iterative coupling algorithm, the evolution of the optimal relaxation parameter and the convergence of the iterative process are briefly illustrated in Fig. 5. In Fig. 5(a), the total amounts of iterative steps necessary for convergence are depicted, for each frequency, considering the spatial discretizations illustrated in Fig. 2.
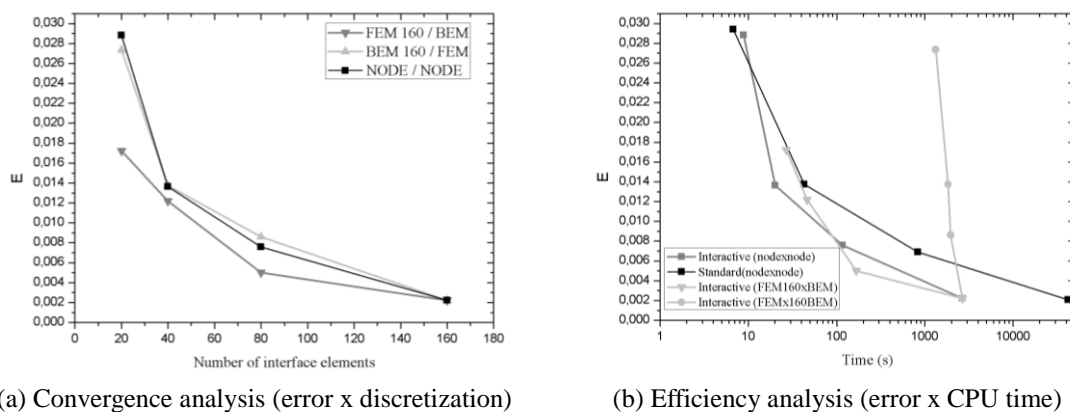

(a) Convergence analysis (error x discretization)   (b) Efficiency analysis (error x CPU time)

Fig. 4 Error analysis

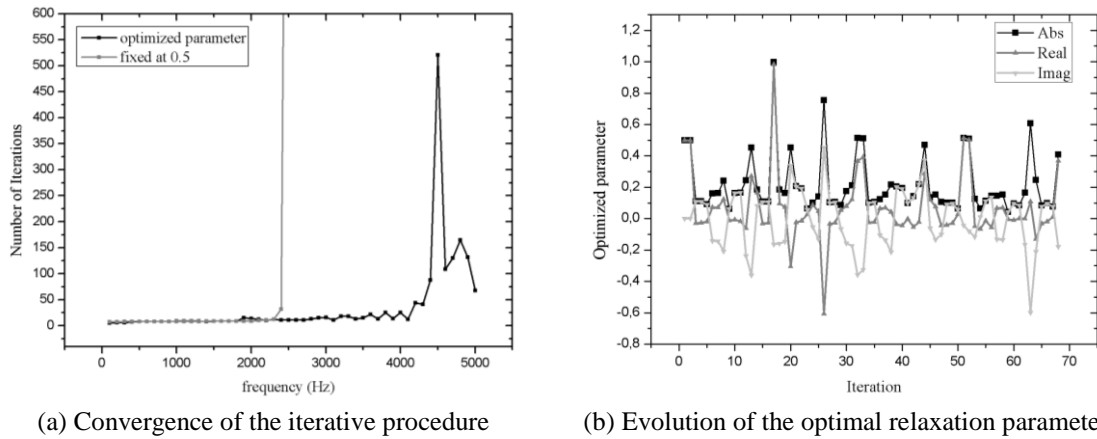(a) Convergence of the iterative procedure   (b) Evolution of the optimal relaxation parameter

Fig. 5 Convergence and optimal relaxation parameter evolution

For comparison, results are also depicted considering a constant relaxation parameter value of 0.5. As one can observe, for higher frequencies (above 2500 Hz), convergence is not achieved if λ = 0.5 is adopted, highlighting the importance of Eq (16) for the effectiveness of the iterative coupling analysis. Moreover, for a constant value λ = 1.0, convergence is never achieved considering the entire adopted frequency range, further illustrating the importance of relaxation parameters in the iterative coupling technique. In Fig. 5(b), the evolution of the optimally computed relaxation parameters (Eq. (16)) are illustrated, taking into account ω = 5000 Hz. As one can observe, its evolution is quite complex since it is based on residuals computed at consecutive iterative steps.

6.2 Concrete tunnel surrounded by soil

Consider, once again, a circular homogeneous ring-shaped elastic structure, inside a homogeneous and infinite soil environment. The external environment is analysed considering two types of materials. First, rock is considered (rigid soil), with density of 1900 kg/m^3, Lamé constant $\mu = 2.5 \times 10^{10}$ N/m^2 and Poisson's ratio of 0.35 (no damping). In the sequence, clay is considered (soft soil), with density of 1300 kg/m^3, Lamé constant $\mu = 1.85 \times 10^5$ N/m^2 and Poisson's ratio of 0.35 (no damping). The first material allows dilatational and shear waves to travel at 7550.99 m/s and 3627.38 m/s, respectively; while the second material allows velocities of $24.83\,m/s$ (dilatational) and $11.93\,m/s$ (shear). The tunnel structure is made of concrete and has an external radius of 3.0 m and an internal radius of 2.0 m. It has a density of 2500 kg/m^3, $\mu = 1.0417 \times 10^{10}$ N/m^2 and Poisson's ratio of 0.2 (no damping). The structure is loaded as indicated in Fig. 6(a), i.e., the load is applied at the bottom of the concrete ring internal cavity, with constant amplitude of 850 kN/m. The corresponding FEM and BEM discretizations are illustrated in Figs. 2(b) and 2(c), respectively. In Figs. 6(b) and 6(c), the computed deformation of the tunnel (rock external environment) is illustrated, considering ω = 500 Hz.

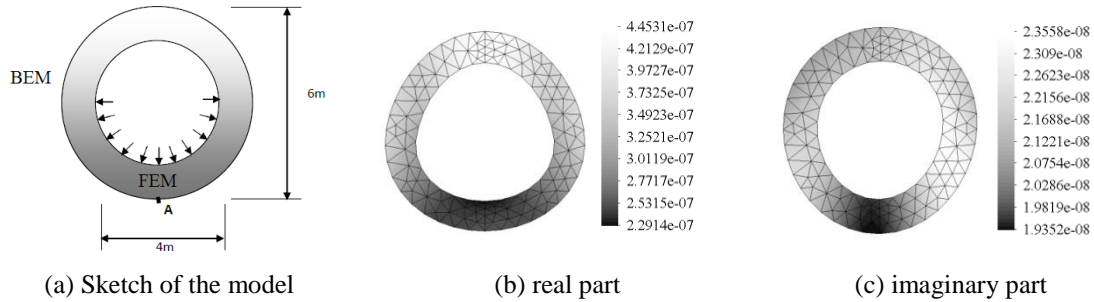(a) Sketch of the model   (b) real part   (c) imaginary part

Fig. 6 Model's sketch and scaled deformation of the tunnel for $\omega = 500$Hz

Fig. 7 illustrates the displacements computed at point A (see Fig. 6(a)), taking into account the proposed iterative and a standard direct FEM-BEM coupling procedure, considering a frequency range from 10 to 500 Hz. As one can observe, the results provided by these different approaches are once again in good agreement, indicating that the iterative solution is converging to the right solution.

(a) Real part (rigid soil)   (b) Imaginary part (rigid soil)
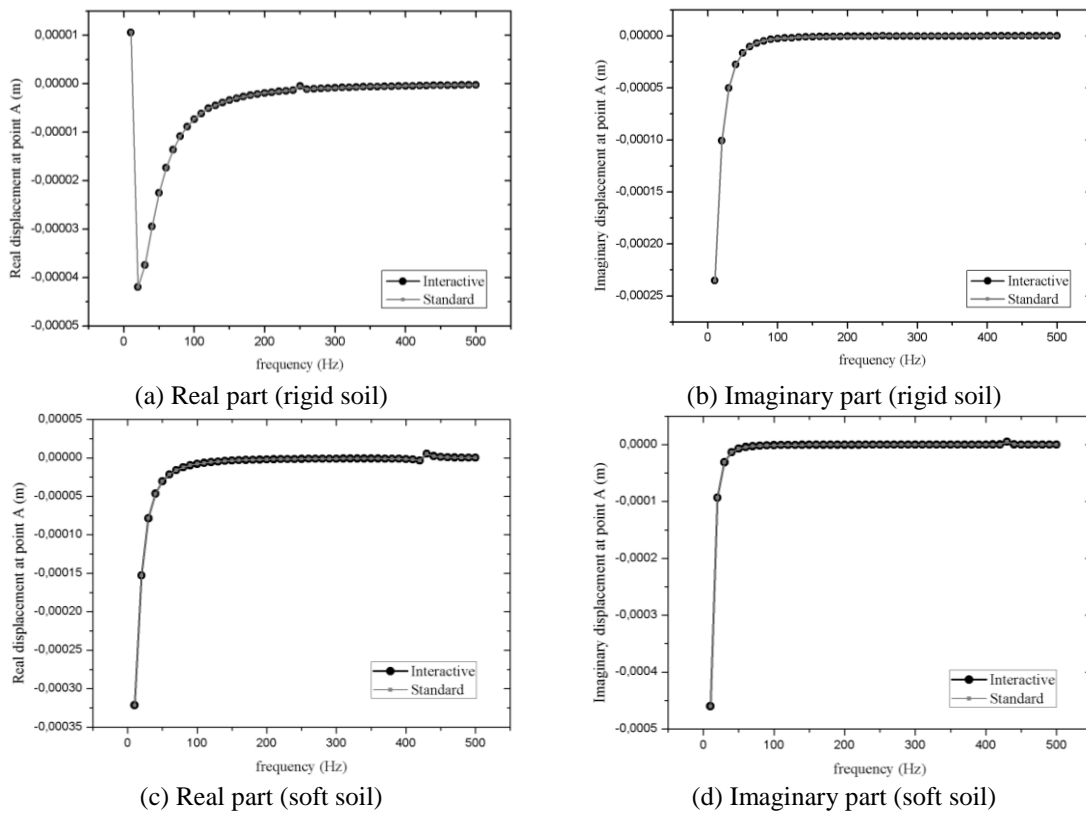

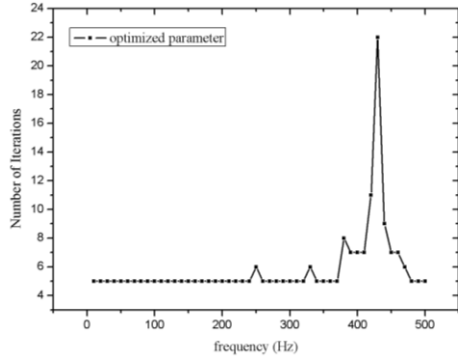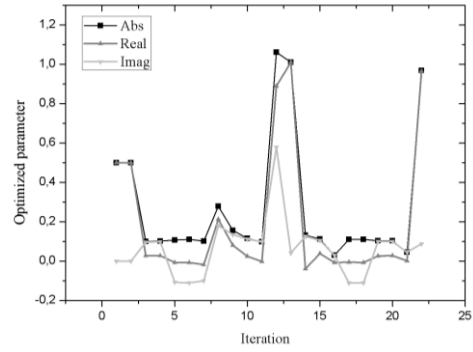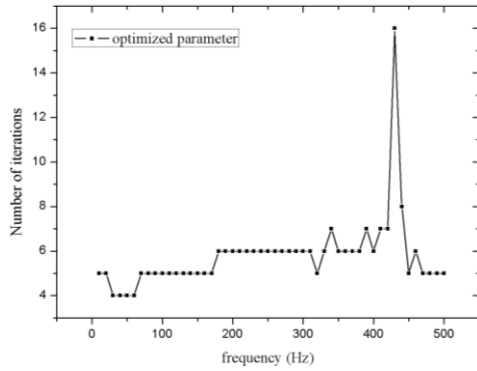(c) Real part (soft soil)   (d) Imaginary part (soft soil)

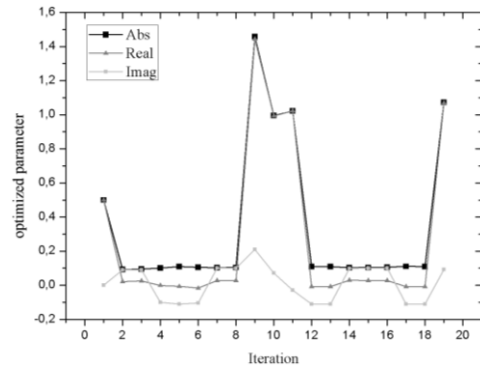Fig. 7 Vertical displacements at point A

(a) Convergence of the iterative procedure (rigid soil)

(b) Evolution of the optimal relaxation parameter (rigid soil)

(c) Convergence of the iterative procedure (soft soil)

(d) Evolution of the optimal relaxation parameter (soft soil)

Fig. 8 Convergence and optimal relaxation parameter evolution

In Figs. 8(a) and 8(c), the total amounts of iterative steps necessary for convergence are depicted, taking into account the selected frequency range. As one can note, for all tested frequencies, convergence occurred with a relatively small amount of iterations, with no more than 25 iterations being necessary at any of the tested frequencies. It is important to highlight that, for the present application, for $\lambda = 0.5$ and $\lambda = 1.0$, convergence is never achieved considering the entire adopted frequency range, further illustrating the importance of optimal relaxation parameters in the iterative coupling technique. In Fig. 8b and 8d, the evolution of the optimally computed relaxation parameters (Eq. (16)) are illustrated for the rigid and soft soil, respectively, taking into account $\omega = 430$ Hz.

7. Conclusions

A FEM-BEM iterative coupling algorithm was discussed here to analyze elastodynamic models, taking into account frequency domain formulations. In order to deal with this ill-posed problem, optimal relaxation parameters were introduced into the iterative coupling analyses, enabling

convergence at a relative low number of iterative steps. An efficient and easy to implement expression to compute the optimal relaxation parameters was discussed and tested, providing an effective and robust iterative coupling procedure.

The use of iterative coupling approaches enables the separated analysis of different sub-domains, leading to better conditioned, smaller and easier to deal with systems of equations, as well as independent definitions of nodal points along distinct sub-domains, allowing non-matching nodes on common interfaces to be easily considered. In section 6 several results were presented, illustrating the versatility and effectiveness of the proposed procedure.

As a matter of fact, the present methodology represents an important step forward in the analyses of wave propagation in frequency domain problems considering iterative coupling procedures, which are well-known ill-posed problems, specially taking into account sub-domains governed by different physical properties and discretized by different numerical techniques.

Acknowledgments

References

Bathe, K.J. (1996), *Finite Element Procedures*, Prentice Hall Inc., New Jersey.

Ben Belgacem, F. (1999), "The mortar finite element methodwith Lagrange multipliers", *Numerische Mathematik*, **84**, 173-197.

Bendali, A., Boubendir, Y. and Fares, M. (2007), "A FETI-like domain decomposition method for coupling finite elements and boundary elements in large-size problems of acoustic scattering", *Comput. Struct.*, **85**(9), 526-535.

Bernardi, C., Maday, Y. and Patera, A.T. (1990), A New Non Conforming Approach to Domain Decomposition: The Mortar Element Method. College de France Seminar, Pitman, H. Brezis, J.–L Lions.

Beskos, D.E. (2003), "Dynamic analysis of structures and structural systems", (Eds., Beskos, D.E. and Maier, G.), *Boundary Element Advances in Solid Mechanics*, CISM International Centre for Mechanical Sciences No. 440, Springer-Verlag, Wien, New York.

Boumaiza, D. and Aour, B. (2014), "On the efficiency of the iterative coupling FEM–BEM for solving the elasto-plastic problems", *Eng. Struct.*, **72**, 12-25

Dominguez, J. (1993), *Boundary elements in dynamics, Computational Mechanics Publications*, Southampton and Boston.

Elleithy, W. (2012), "Multi-region adaptive finite element-boundary element method for elasto-plastic analysis", *Int. J. Comput.Math.*, **89**(11), 1525-1539.

Elleithy, W.M., Al-Gahtani, H.J. and El-Gebeily, M. (2001), "Iterative coupling of BE and FE methods in elastostatics", *Eng. Anal. Bound. Elem.*, **25**(8), 685-695.

Elleithy, W. and Grzhibovskis, R. (2009), "An adaptive domain decomposition coupled finite element– boundary element method for solving problems in elasto-plasticity", *Int. J. Numer. Meth. Eng.*, **79**, 1019-1104.

Godinho, L. and Soares, D. (2013), "Frequency domain analysis of interacting acoustic-elastodynamic models taking into account optimized iterative coupling of different numerical methods", *Eng. Anal. Bound. Elem.*, **37**, 1074-1088.

Gosselet, P. and Rey, C. (2006), "Non-overlapping domain decomposition methods in structural mechanics", *Arch. Comput. Meth. Eng.*, **13**(4), 515-572.

Hughes, T.J.R. (2000), *The Finite Element Method – Linear Static and Dynamic Finite Element Analysis*, Dover Publications, New York.

Jahromi, H.Z., Izzuddin, B.A. and Zdravkovic, L. (2009), "A domain decomposition approach for coupled modelling of nonlinear soil-structure interaction", *Comput. Method. Appl. M.*, **198**(33-36), 2738-2749.

Lin, C.C., Lawton, E.C., Caliendo, J.A. and Anderson, L.R. (1996), "An iterative finite element-boundary element algorithm", *Comput. Struct.*, **59**(5), 899-909.

Soares, D. (2008), "An optimised FEM-BEM time-domain iterative coupling algorithm for dynamic analyses", *Comput. Struct.*, **86**(19-20), 1839-1844.

Soares, D. (2012), "FEM-BEM iterative coupling procedures to analyze interacting wave propagation models: fluid-fluid, solid-solid and fluid-solid analyses", *Coupled Syst. Mech.*, **1**(1), 19-37.

Soares, D. and Godinho, L. (2012), "An optimized BEM-FEM iterative coupling algorithm for acoustic-elastodynamic interaction analyses in the frequency domain", *Comput. Struct.*, **106-107**, 68-80.

Soares, D. and Godinho, L. (2014), "An overview of recent advances in the iterative analysis of coupled models for wave propagation", *J. Appl. Math.*, **2014**, Article ID 426283.

Soares, D., von Estorff, O. and Mansur, W.J. (2004), "Iterative coupling of BEM and FEM for nonlinear dynamic analyses", *Comput. Mech.*, **34**, 67-73.

Vion, A. and Guezaine, C. (2014), "Double sweep preconditionner for optimized Scwarz methods applied to Helmholtz problem", *J. Comput. Phys.*, **266**, 171-190.